Title: Molecular and cellular similarities in the brain of SARS-CoV-2 and Alzheimer's disease individuals

Authors: Elizabeth Griggs,[1] Kyle Trageser,[1] Sean Naughton,[1] Eun-Jeong Yang, [1] Brian Mathew,[1] Grace Van Hyfte,[1] Linh Hellmers,[3] Nathalie Jette,[1] Molly Estill,[1] Li Shen,[1] Tracy Fischer,[3,4] Giulio Maria Pasinetti[1,2]*

Affiliations:

[1]Department of Neurology, Icahn School of Medicine at Mount Sinai, New York, New York, USA.

[2]Geriatric Research, Education and Clinical Center, James J. Peters Veterans Affairs Medical Center, Bronx, New York, USA.

[3]Tulane National Primate Research Center, Covington, Louisiana, USA.

[4]Department of Microbiology and Immunology, Tulane University School of Medicine, New Orleans, Louisiana, USA.

*To whom correspondence should be addressed:

Giulio Maria Pasinetti, M.D., Ph.D.

Department of Neurology

The Mount Sinai School of Medicine

1 Gustave L. Levy Place, Box 1137

New York, NY 10029

Phone: (212) 241-7938

Fax: (212) 876-9042

Email: giulio.pasinetti@mssm.edu

Abstract

Infection with the etiological agent of COVID-19, SARS-CoV-2, appears capable of impacting cognition, which some patients with Post-acute Sequelae of SARS-CoV-2 (PASC). To evaluate neuro-pathophysiological consequences of SARS-CoV-2 infection, we examine transcriptional and cellular signatures in the Broadman area 9 (BA9) of the frontal cortex and the hippocampal formation (HF) in SARS-CoV-2, Alzheimer's disease (AD) and SARS-CoV-2 infected AD individuals, compared to age- and gender-matched neurological cases. Here we show similar alterations of neuroinflammation and blood-brain barrier integrity in SARS-CoV-2, AD, and SARS-CoV-2 infected AD individuals. Distribution of microglial changes reflected by the increase of Iba-1 reveal nodular morphological alterations in SARS-CoV-2 infected AD individuals. Similarly, HIF-1α is significantly upregulated in the context of SARS-CoV-2 infection in the same brain regions regardless of AD status. The finding may help to inform decision-making regarding therapeutic treatments in patients with neuro-PASC, especially those at increased risk of developing AD.

Teaser

SARS-CoV-2 and Alzheimer's disease share similar neuroinflammatory processes, which may help explain neuro-PASC.

Introduction

The consequences of SARS-CoV-2 infection have been well-studied in the respiratory system; however, much less information is available regarding the neurological consequences of infection (*1*). Previous evidence tentatively suggests that SARS-CoV-2 may be neuroinvasive, leading to a vast array of neurological symptoms, including anosmia, ageusia, cognitive functions, and cerebrovascular disorders (*2*, *3*). Neurological complications of SARS-CoV-2 infection manifest with increased severity related to age and shared medical history of metabolic disorders and other vascular risk factors (*4*–*6*). Some strains within the coronavirus family are implicated in neuronal degeneration such as HCoV-OC43, which can lead to glutamate excitotoxicity and neuronal degradation in mice through cytokine production (*7*, *8*). Because SARS-CoV-2 is a new addition to the coronavirus family, little information exists regarding potential long-term neurological complications that may impact COVID-19 survivors. This may be especially concerning for aging individuals with increased vulnerability to developing age-related neurodegenerative disease.

While it is currently unknown if neurological manifestations of SARS-CoV-2 infection arise solely from systemic inflammation in the periphery or brain infiltration, it is well established that secretion of cytokines and chemokines from the periphery allows the recruitment of leukocytes and other cells to specific tissues (*9*, *10*). This type of immune response is speculated to accelerate blood-brain barrier (BBB) disruption and may potentially damage cells within the central nervous system (CNS) (*11*). Such effects are similar to neuropathology seen in Alzheimer's disease (AD) and other neurodegenerative disorders, where leukocyte infiltration, BBB dysregulation, and microglial activation are observed. Thus, it is possible that SARS-CoV-2 may accelerate the onset and severity of

cognitive decline or AD in susceptible individuals (*12*, *13*). Understanding the impact of SARS-CoV-2 infection on the CNS and subsequent mechanisms associated with cognition is particularly pressing, given the number of individuals presenting with neurological symptoms of post-acute sequelae of SARS-CoV-2 (neuro-PASC), colloquially termed 'long-COVID' (*14*, *15*).

Here, we investigate potential brain mechanisms associated with SARS-CoV-2 infection in SARS-CoV-2, AD and SARS-CoV-2 infected AD individuals by comparing transcriptional and cellular responses in the cortical Broadman area 9 (cortical BA9) of the frontal cortex and the hippocampal formation (HF); two brain regions deeply involved in cognitive and emotional functions, to age- and gender-matched neurological cases. Here we report evidence suggesting that SARS-CoV-2 infection promotes similar pathophysiological features found in AD cortical BA9 and HF regions and possibly exacerbate pre-existing AD pathophysiology.

Results

Demographics of human postmortem cases

We examined postmortem tissue samples of cortical Broadman area 9 (cortical BA9) of the frontal cortex and the hippocampal formation (HF) collected by the Neuropathology Brain Bank and Research CoRE at Mount Sinai from 4 different groups: SARS-CoV-2, AD, and AD individuals which became infected by SARS-CoV-2, compared to age- and gender-matched neurological cases (Table S1). Each group comprises an equal number of age-matched male and female patients, ensuring equal distribution with an average age of 79.6 among groups. Medical records indicate that all AD individuals have postmortem ABC scores indicative of AD (Table S2), where A is a measure of amyloid beta

deposition, B is a measure of neurofibrillary degeneration based on the Braak and Brook score, and C is scored based on neuritic plaques outlined by the Consortium to Establish a Registry for Alzheimer's Disease diagnosis (CERAD) (*16*). SARS-CoV-2 infection was confirmed by diagnostic polymerase chain reaction (PCR). Within the SARS-CoV-2 and SARS-CoV-2 infected AD groups, all patients were symptomatic, admitted to the hospital, and received oxygen supplementation by ventilator or cannula with disease onset to death occurring on average, 27 days after diagnosis for patients with SARS-CoV-2 only and 32 days after diagnosis in infected AD patients (Table S1 and S2). Blood specimens were collected and indicate several laboratory features of severe COVID-19 (Table S2), such as increased C-reactive protein (CRP) and interleukin-6 (IL-6) (*17*).

Gene expression of SARS-CoV-2 and AD groups compared to control cases in cortical BA9 and HF tissues

The transcriptional profiles of AD and SARS-COV-2 infected postmortem cases from the cortical BA9 were assessed by pairwise comparison to determine gene expression compared to neurological control cases (**Fig. 1A-C**). Volcano plot distributions of gene transcripts of SARS-CoV-2 and AD cases compared to neurological controls (**Fig. 1A**, **B**) both reveal 39,901 genes which were used to determine differentially expressed genes based on a nominal p-value less than 0.01 and an absolute log fold-change (logFC) greater than 1. We find in the AD group, 287 genes are upregulated, and 131 genes are downregulated. In the SARS-CoV-2 group, 179 genes are upregulated, and 426 genes are downregulated. The Volcano plot distribution of gene transcripts of SARS-CoV-2 infected AD cases compared to neurological controls (**Fig. 1C**) revealed from 38,021 genes, and show 813 genes upregulated, 611 genes downregulated using the same cutoff for significance as in (**Fig. 1A, B**).

Transcriptional profiles of AD and SARS-COV-2 cases from the HF were assessed ($p<0.01$ and $logFC>1$) to determine gene expression, as compared to neurological control cases **(Fig. 1D-F)**, using 39,901 genes for SARS-CoV-2 and AD cases (**Fig. 1D, E**), and 35,527 genes for the SARS-CoV-2 infected AD cases (**Fig. 1F**). We find in the AD group, 304 genes upregulated, 214 genes downregulated. In the SARS-CoV-2 group, 230 genes are upregulated, and 464 genes are downregulated. Additionally, in the SARS-CoV-2 infected AD group 466 genes upregulated, 582 genes downregulated.

Similarity of gene expression in cortical BA9 and HF regions

In order to determine the relative similarity of gene expression changes induced by disease state, a collection of genes known to be differentially expressed due to either SARS-CoV-2 infection or AD were examined across three individual differential comparisons (**Fig. 2A, 2B**). While all three comparisons (AD versus Control, SARS-CoV-2 versus Control, and SARS-CoV-2 infected AD versus Control) showed generally the same trends, the AD and SARS-CoV-2 infected AD comparisons were strikingly similar, in both BA9 (**Fig. 2A**) and HF (**Fig. 2B**).

Rank-rank hypergeometric overlap (RRHO) analysis comparing SARS-CoV-2 and AD cases also reveals a positive correlation between the AD and SARS-CoV-2 groups in the cortical BA9 (Fig. S1) as well as in the HF (Fig. S2), although to a lesser extent than in the cortical BA9. We then filtered genes using Ingenuity Pathway Analysis software (IPA) to determine the number of shared differentially regulated genes among the SARS-CoV-2, AD, and SARS-CoV-2 infected AD groups within each tissue region ($p<0.05$ and absolute $z > 0.0001$). Comparing these shared genes within the cortical BA9, we find that SARS-

CoV-2, AD and SARS-CoV-2 infected AD individuals shared 410 upregulated genes, 269 downregulated genes from 679 expressed genes (**Fig. 2C**; Data S1). In the HF we found the three groups share 211 upregulated genes, 148 downregulated genes from 359 differentially expressed genes (**Fig. 2D**; Data S2).

Pathway activation of SARS-CoV-2 and AD groups

IPA was employed to further characterize pathways in SARS-CoV-2, AD and SARS-CoV-2 infected AD groups compared to the neurological controls. Within the cortical BA9 region (**Fig. 3A**), for example several pathways such as neuroinflammation, TREM1, and cell senescence show increased activation in the SARS-CoV-2, AD and SARS-CoV-2 infected AD groups. TREM1 signaling, the most highly activated pathway in this dataset **(Fig. 3A, B),** is expressed primarily on myeloid cells, such as macrophages and microglia, and is involved in pro-inflammatory immune responses (*18*). Although cellular senescence due to age is a natural process where telomeres shorten over time, this process also occurs during cellular stress due to inflammation, including from viral infections, leading to a senescence-associated secretory phenotype (SASP) such as metalloproteinases (MMP's), and inflammatory cytokines (*19, 20*) (**Fig. 3A**). Another pathway of interest, SNARE, shows decreased activation in AD and SARS-CoV-2 groups (**Fig. 3A**), with the most significant reduction seen in the SARS-CoV-2 infected AD cases group. SNARE proteins play an essential role in neurotransmitter release, and altered function is implicated in the pathophysiology of neurodegenerative diseases such as AD, where SNARE proteins affect β-amyloid (Aβ) accumulation and cytoplasmic transport of neurofibrillary tangles (*21*).

Within the HF (**Fig. 4A**), for example interleukin-8 (IL-8) another neuroinflammatory pathway, and ciliary neurotrophic factor (CNTF) signaling is upregulated in SARS-CoV-2, AD and SARS-CoV-2 infected AD groups, while cAMP response element-binding protein (CREB) is also upregulated in SARS-CoV-2 groups but downregulated in AD-only (**Fig. 4A**). IL-8 has several important roles, including endothelial cell migration and chemoattraction of neutrophils (*22*). One way IL-8 aids cell migration is by enhancing the expression of molecules such as MMP-2, MMP-9, involved in BBB integrity and induction of neuronal apoptosis, and VEGF-A, involved in vascular permeability and angiogenesis, thus having a potential effect on vascular damage (*23–25*). CNTF signaling aids in the prevention of neuronal degeneration after injury and is neuroprotective in diseases such as multiple sclerosis (MS) and amyotrophic lateral sclerosis (ALS) (*26*). Interestingly, CREB signaling modulates processes in consolidating memory and information processing and is inhibited in AD (*27*). Consistent with these findings, we also see a reduction in CREB signaling in the AD individuals; however, this effect is reversed in SARS-CoV-2 infected AD individuals in the HF. It is important to note that TREM1 signaling is upregulated in two of the three sample groups (SARS-CoV-2 and SARS-CoV-2 infected AD cases), but no predictions for this pathway occurs in the AD group. As such, this pathway is not included in the analysis within the HF (**Fig 4A,B**).

Additionally, upregulation of integrin signaling and nerve growth factor (NGF) signaling occur in both cortical BA9 and HF tissue **(Fig's. 3B and B4)** in all SARS-CoV-2, AD and SARS-CoV-2 infected AD groups. Neuronal function shown by the upregulation of NGF signaling is critical for the survival of neurons, and alterations of NGF signaling has been implicated in neurodegenerative disorders such as AD (*28*). Integrin signaling is used for a

diverse array of functions within the CNS via cell-to-cell and cell-to-extracellular matrix interactions (*29*).

Regulation of inflammatory microglia responses in cortical BA9 and HF sections

Region-matched formalin-fixed paraffin-embedded (FFPE) tissue from the contralateral hemisphere of cortical BA9 and HF used for transcriptional studies underwent immunohistochemical (IHC) analysis for evidence of microglial activation (Iba-1), the presence of SARS-CoV-2 (SARS-CoV-2 nucleocapsid), and vascular integrity, assessed via hypoxia-inducible factor-1α subunit (HIF-1α).

Neuroinflammation was assessed with a pan-microglia marker, Iba-1, which is upregulated by microglia in the context of inflammation and reveals morphological alterations associated with their activation state (**Fig. 5**). Compared to neurological controls, microglia in AD, SARS-CoV-2, and SARS-CoV-2 infected AD cases are more numerous and display an activated phenotype, with retracted, thickened processes and enlarged somas (**Fig. 5 A-D**). Microglia also appear to accumulate around blood vessels in the context of AD and SARS-CoV-2 groups but not in unaffected neurological controls brain (**Fig. 5 E-H**), suggesting factors at the level of the BBB may participate in microglial activation. Microglial nodules, which are commonly observed in neuroinflammatory disease, were seen in all conditions but appeared larger and more frequently in infection, as compared to AD-only and controls (**Fig. 5 I-L**). When detectable, SARS-CoV-2 appears to be restricted to the endothelium (**Fig. 5 G, H, K, L**) and did not colocalize with Iba-1 or glial fibrillary acidic protein (GFAP; data not shown), suggesting neither microglia nor astrocytes harbor productive virus. Nonbiased quantitation revealed an overall increase in the number of microglia in the HF and cortical

BA9 of patients with AD, SARS-CoV-2, and SARS-CoV-2 infected AD cases. A statistically significant increase in the number of microglia occurs in AD alone in the HF and SARS-CoV-2 infected AD cases in both the HF and cortical BA9 (**Fig. 5**). An increase in the frequency of nodular lesions was seen with SARS-CoV-2 infection, with and without AD, in both brain regions assessed. However, a statistically significant increase in nodular lesions are present in SARS-CoV-2 infected AD cases (**Fig. 5P-R**).

Regulation of vascular damage using hypoxia inducible factor- 1α (HIF-1α) detection

Tissues were further assessed for possible hypoxia by IHC using an antibody against the α subunit of HIF-1, which is stabilized under hypoxic conditions. Upregulation and stabilization of HIF-1α is most pronounced in the context of SARS-CoV-2 infection, regardless of AD status in cortical BA9 (**Fig. 6A-D**) and HF (**Fig. 6E-H**). Nonbiased area positivity quantitation revealed HIF-1α is only slightly elevated in cortical BA9 of AD patients, as compared to age-matched neurological controls (**Fig. 6J**). In contrast, a greater increase occurs in the HF from SARS-CoV-2 individuals, with and without AD. SARS-CoV-2 only samples showed a significant increase in HIF-1α of cortical BA9 when compared to controls (**Fig. 6I-K**).

Discussion

The finding from our study suggests that SARS-CoV-2 and AD infected individuals share similar alterations of regulatory patterns of immune-inflammatory pathways and pathways involved with cognition as suggested by recent meta-analyses showing shared neuroinflammation and microvascular injury, in particular AD and SARS-CoV-2 infected individuals (*30*). Additionally, Zhou and colleagues found a significant overlap in cerebrospinal fluid (CSF) monocytes and markers in AD and COVID-19, which also

246 occurs in our dataset (*30*). The similarities of transcriptional profiles and cellular
247 pathophysiology in SARS-CoV-2 and SARS-CoV-2 infected individuals support the
248 potential role of SARS-CoV-2 infection on the CNS, leading to neuro-PASC symptoms
249 such as brain fog and memory loss.
250
251 Notably, our study identifies similar neuroinflammatory profiles in SARS-CoV-2, AD and
252 AD SARS-CoV-2 infected individuals at the transcriptional and cellular levels in both the
253 cortical BA9 and HF brain regions. This suggests that SARS-CoV-2 generates a similar
254 neuroinflammatory environment in neurodegenerative disorders like AD. This was
255 highlighted by the regulation of TREM1, neuroinflammation, and cellular
256 senescence/inflammatory pathways present in all groups and further established by the
257 widespread microglial activation seen in AD and SARS-CoV-2 infected AD cases, and in
258 particular, the nodular formation seen in SARS-CoV-2 infected AD cases. Microglia
259 nodule formation is present in some neurodegenerative diseases, such as MS, and viral
260 infections, such as herpes simplex virus (HSV) and human immunodeficiency virus (HIV)
261 (*31, 32*). A potentially compounding finding is the nodular formation that is initially
262 characterized by abundant presence of activated microglia and innate immune factors
263 leading to toll-like receptor (TLR) signaling and upregulations of inflammasome genes,
264 leading to T cell stimulation and ultimately the destruction of neurons (*31*). This may be
265 of particular concern in the SARS-CoV-2 infected AD cases, where we primarily observe
266 increased nodular lesions. This suggests SARS-CoV-2 further promotes
267 neuroinflammation in AD, which likely advances the progression and severity of CNS
268 disease in these individuals. Interestingly, a large retrospective study of patients 65 years
269 or older revealed that patients with SARS-CoV-2 were at an increased risk for a new AD
270 diagnosis within a year of their SARS-CoV-2 diagnosis, with the most significant risk

seen among those 85 years and older (*33*). This may underscore the critical role of preexisting inflammation in the brain, which is seen in the context of 'normal' aging, in promoting or advancing AD progression.

Our findings also support the notion that SARS-CoV-2 may cause cognitive deficits via regulation of pathways associated with cognition and neuroinflammation. Here, we show changes in the transcriptional regulation of SNARE and NGF pathways, suggesting impaired neuronal health and function, presumably negatively impacting cognitive function. We also observed potential damage to the vasculature via increased regulation of HIF-1α, integrin signaling, and IL-8 signaling. It is important to note a possibility of vascular damage due to ventilation prior to death in SARS-CoV-2 infected individuals; however, vascular damage by SARS-CoV-2, as assessed by HIF-1α, is observed in non-human primates that were euthanized at designated end-of-life time points precluding breathing intervention (*34*). These findings may point to a possible route for lymphocyte transmigration following chemoattractant gradients such as IL-8 and enhancement of MMPs and VEGF, which are aided by integrins such as cellular adhesion molecules such as ICAM-1 and are implicated with inflammatory signal transduction (*35*, *36*). This process leads to T cell activation, which may be responsible for the observed inflammatory environment. Our transcriptional data showed an abundant upregulation of TLRs (TLRs 1, 5, 7, and 8) related to the inflammasome. Further analysis of this dataset also indicated the potential role for T cells through IL-7 pathway activation and CD86 upregulation; however, we did not confirm changes in the number of T cells, and no evidence of leukocyte infiltration into the CNS compartment was observed in any disease state in this investigation. Future studies will be required to determine the role of leukocytes in the observed pathophysiology.

Although neuroinflammation and vascular injury were prominent features of SARS-CoV-2 and SARS-CoV-2 infected AD cases brain pathology, the direct role of the virus is unclear. We did detect SARS-CoV-2 nucleocapsid in some SARS-CoV-2 brain tissues that appear to be restricted to the vasculature. This finding is supported by other studies suggesting SARS-CoV-2 is sporadically present in brain tissue (*37*). Importantly, we only investigated CNS regions with the greatest significance in AD. These regions may be less prone to SARS-CoV-2 infection than others, such as the olfactory bulb and tract, where olfactory neurons are proposed to be infected through viral spread from olfactory epithelium (*38*). Our findings of the viral nucleocapsid limited to the endothelium suggest the hematological spread of SARS-CoV-2 to the CNS that may not extend to the neurons in the cortical BA9 and HF yet is still capable of inducing widespread inflammation in the brain.

Even in the absence of a detectable virus in the neurons or neural cells, SARS-CoV-2 may impact cognitive dysfunction through TREM1 activation of the NLRP3 inflammasome and subsequent pyroptosis, where pro-caspase 1 cleavage and subsequent cleavage and activation of IL-1β, IL-18 and gasmerdin D pore formation in cells ultimately leading to pyroptosis (*39*, *40*). NLRP3 activation is reported in AD and COVID-19, and is suggested by formation of microglial nodules demonstrated in these cases (*41–43*).`

SARS-CoV-2 is not the first virus to be implicated in cognitive dysfunction. This is a facet shown with other viruses such as HIV, HSV, and Epstein-Barr virus (EBV) (*44*, *45*). While this study cannot predict the outcome of disease progression in COVID-19

survivors, the present findings that SARS-CoV-2 infection can recapitulate AD-type transcriptional and cellular neuroinflammatory patterns among other in a very short time frame makes it critical to understand how SARS-CoV-2 impacts long-term cognition. The increase in nodular formation present in SARS-CoV-2 infected AD cases tissue also demonstrates a critical need to functionally determine potentially synergistic effects of AD and SARS-CoV-2. This is underscored by the prevalence of cognitive dysfunction seen among neuro-PASC patients, making it imperative that the link between SARS-CoV-2 and cognition be intensively investigated to identify potential therapeutic strategies for halting cognitive decline in these individuals. Collectively, our results demonstrate several key areas of overlap between the neurological effects of SARS-CoV-2 infection and AD. These findings may help inform decision-making regarding therapeutic treatments in patients with COVID-19, especially those who may be at increased risk of developing AD.

Materials and Methods

Patients

Brain tissue was collected from the cortical BA9 region (cortical BA9) and hippocampal formation (HF) of four SARS-CoV-2 cases, four Alzheimer's disease (AD) cases and four non-SARS-CoV-2 or AD autopsies. With each case, one hemisphere of the brain was formalin-fixed paraffin-embedded (FFPE) and the other hemisphere was frozen to generate fresh-frozen blocks. FFPE tissue was used for microscopy and region matched fresh-frozen tissue was used for sequencing.

Tissue was collected in accordance with IRB-approved guidelines and regulations by the Brain Bank at Mount Sinai, and clinical data including cardiovascular and neurological conditions were collected by the Department of Neurology.

346 **RNA sequencing**

347 Samples collected and homogenized in RNAzol RT (Molecular Research Center, Inc.)
348 were then processed using the Zymo Clean and concentrator Kit (Zymo Research) to
349 collect total RNA following the manufacturers protocols. cDNA library construction and
350 sequencing were conducted by Genewiz (Azenta Life Sciences). Total RNA samples were
351 quantified using Qubit 2.0 Fluorometer (Life Technologies, Carlsbad, CA, USA) and
352 RNA integrity was checked with 4200 TapeStation (Agilent Technologies, Palo Alto, CA,
353 USA).

354

355 Samples were treated with TURBO DNase (Thermo Fisher Scientific, Waltham, MA,
356 USA) to remove DNA contaminants, followed by rRNA depletion using QIAseq®
357 FastSelect™–rRNA HMR kit (Qiagen, Germantown, MD, USA); conducted following
358 the manufacturer's protocol. RNA sequencing libraries were constructed with the
359 NEBNext Ultra II RNA Library Preparation Kit for Illumina by following the
360 manufacturer's recommendations, where enriched RNAs were fragmented for 15 minutes
361 at 94 °C. First strand and second strand cDNA are subsequently synthesized. cDNA
362 fragments are end repaired and adenylated at 3'ends, and universal adapters are ligated to
363 cDNA fragments, followed by index addition and library enrichment with limited cycle
364 PCR. Sequencing libraries were validated using the Agilent Tapestation 4200 (Agilent
365 Technologies, Palo Alto, CA, USA), and quantified using Qubit 2.0 Fluorometer
366 (ThermoFisher Scientific, Waltham, MA, USA) as well as by quantitative PCR (KAPA
367 Biosystems, Wilmington, MA, USA). The sequencing libraries were multiplexed and
368 clustered on one lane of a flowcell. After clustering, the flowcell was loaded on the
369 Illumina HiSeq 4000 instrument according to manufacturer's instructions. The samples
370 were sequenced using a 2x150 Pair-End (PE) configuration.

Image analysis and base calling were conducted by the HiSeq Control Software (HCS). Raw sequence data (.bcl files) generated from Illumina HiSeq was converted into FASTQ files and de-multiplexed using Illumina's bcl2fastq 2.17 software. One mismatch was allowed for index sequence identification. After investigating the quality of the raw data, sequence reads were trimmed to remove possible adapter sequences and nucleotides with poor quality using Trimmomatic v.0.36. The trimmed reads were mapped to the GRCh38 reference genome available on ENSEMBL using the STAR aligner v.2.5.2b. BAM files were generated as a result of this step. Unique gene hit counts were calculated by using feature Counts from the Subread package v.1.5.2. Only unique reads that fell within exon regions were counted.

Immunohistochemistry

Tissue was cut at 6 µm on a Leica Microtome to for immunohistochemistry that was performed formalin-fixed paraffin-embedded (FFPE) brain sections as previously described (*46*) (Iba-1 staining was conducted on a Ventana Benchmark using OptiView and UltraView detection kits provided by Roche (Roche Molecular Systems, Inc). Sections were deparaffinized in xylene and rehydrated through an ethanol series ending in distilled water. Heat-mediated antigen retrieval was carried out in a vacuum oven with Tris-EDTA buffer (10mM Trizma base, 1mM EDTA, 0.05% Tween 20, pH 9.0) or sodium citrate buffer (10mM sodium citrate, 0.05% Tween 20, pH 6.0). All washes were performed using tris buffered saline containing Tween 20 (TTBS; 0.1M Trizma base, 0.15M NaCl, 0.1% Tween 20, pH 7.4). Following antigen retrieval, tissues were blocked with 20% normal horse serum. Titrated primary antibodies included anti-HIF-1α (mouse mgc3, 1:400, Abcam, ab16066). Tissues were incubated with primary antibody overnight

at room temperature and detected using the appropriate biotinylated secondary antibody (1:200, Vector Labs, BA-1100, BA-2000) and alkaline phosphatase-Vector Red according to manufacturer instructions (Vector Labs). Tissues were counterstained with Mayer's hematoxylin and coverslipped.

Imaging and quantitation

Slides were scanned with the Axio Scan.Z1 digital slide scanner (Zeiss). Brightfield images were acquired using HALO (Indica Labs, v3.4.2986.151). Figures were created in Photoshop (Adobe, v23.5.1) by brightness and contrast adjustments applied to the entire image.

Threshold and multiplex analyses were performed with HALO algorithms for non-biased quantitation of proteins of interest without processing, as described previously (38). For microglia quantitation, hematoxylin-stained nuclei were used to quantify the total number of cells and those with Vector Red intensity above a rigorous threshold (Iba-1+). Microglia frequency is reported as the percentage of total nuclei in the tissue section assessed. To assess frequency of nodular lesions, all Iba-1-stained tissues were viewed in HALO and nodular lesions made up of 3 or more Iba-1+ microglia in contact with one another were counted as a single nodule. The total number of nodules for each tissue is reported per tissue area. Quantitation of HIF-1α was performed using an area quantification algorithm for Vector Red intensity. Annotations were drawn to outline the tissue and exclude empty spaces and glass. The annotated area was analyzed for overall quantity of Vector Red positivity per micron^2 of tissue. Two-tailed Mann-Whitney U tests were performed with GraphPad Prism software, v9.3.1. Data are expressed as mean ± SEM. P values ≤ 0.05 are considered significant.

421

422 **Bioinformatics Data Access and Analysis**

423 Sample similarity was assessed with PCA analysis on VST-transformed expression values.
424 Genes were filtered to remove lowly expressed genes, defined as fewer than 5 samples
425 showing a minimum read count of 1 read, prior to performing differential analysis with
426 DESeq2, in R (4.2.0) (*47*). The transcriptional profiles of SARS-CoV-2 and AD
427 postmortem cases from the cortical BA9 and HF were assessed by pairwise comparison to
428 the neurologically healthy control cases. Genes were assigned as differentially expressed
429 if the nominal p-value was less than 0.05 and the absolute log2FC exceeded 1. An
430 additional round of differential expression testing was performed using a model containing
431 covariates (COVID status, Alzheimer's status, gender, and brain region), to extract the
432 transcriptional effects of the individual covariates. Biological pathways and key regulators
433 impacted by disease were identified using QIAGEN Ingenuity Pathway Analysis (IPA)
434 (QIAGEN Inc., Version 73620684) (*48*) Genes with a threshold of $p<0.05$ were used as
435 input for IPA. The relative similarities of transcriptional changes in the DESeq2
436 comparisons were assessed using Rank-rank hypergeometric overlap (RRHO2) analysis.

437

438

References

1. T. Flerlage, D. F. Boyd, V. Meliopoulos, P. G. Thomas, S. Schultz-Cherry, Influenza virus and SARS-CoV-2: pathogenesis and host responses in the respiratory tract. *Nat Rev Microbiol*. **19**, 425–441 (2021).

2. M. Desforges, A. Le Coupanec, J. K. Stodola, M. Meessen-Pinard, P. J. Talbot, Human coronaviruses: viral and cellular factors involved in neuroinvasiveness and neuropathogenesis. *Virus Res*. **194**, 145–158 (2014).

3. K. S. Hingorani, S. Bhadola, A. M. Cervantes-Arslanian, COVID-19 and the Brain. *Trends in Cardiovascular Medicine* (2022), doi:10.1016/j.tcm.2022.04.004.

4. A. A. Divani, S. Andalib, J. Biller, M. Di Napoli, N. Moghimi, C. A. Rubinos, C. O. Nobleza, P. N. Sylaja, M. Toledano, S. Lattanzi, L. D. McCullough, S. Cruz-Flores, M. Torbey, M. R. Azarpazhooh, Central Nervous System Manifestations Associated with COVID-19. *Curr Neurol Neurosci Rep*. **20**, 60 (2020).

5. S. H.-Y. Chou, E. Beghi, R. Helbok, E. Moro, J. Sampson, V. Altamirano, S. Mainali, C. Bassetti, J. I. Suarez, M. McNett, GCS-NeuroCOVID Consortium and ENERGY Consortium, Global Incidence of Neurological Manifestations Among Patients Hospitalized With COVID-19—A Report for the GCS-NeuroCOVID Consortium and the ENERGY Consortium. *JAMA Network Open*. **4**, e2112131 (2021).

6. B. N. Sullivan, T. Fischer, Age-Associated Neurological Complications of COVID-19: A Systematic Review and Meta-Analysis. *Frontiers in Aging Neuroscience*. **13** (2021) (available at https://www.frontiersin.org/articles/10.3389/fnagi.2021.653694).

7. H. Jacomy, J. R. St-Jean, É. Brison, G. Marceau, M. Desforges, P. J. Talbot, Mutations in the spike glycoprotein of human coronavirus OC43 modulate disease in BALB/c mice from encephalitis to flaccid paralysis and demyelination. *J Neurovirol*. **16**, 279–293 (2010).

8. E. Brison, H. Jacomy, M. Desforges, P. J. Talbot, Glutamate Excitotoxicity Is Involved in the Induction of Paralysis in Mice after Infection by a Human Coronavirus with a Single Point Mutation in Its Spike Protein. *Journal of Virology*. **85**, 12464–12473 (2011).

9. L. Bauer, B. M. Laksono, F. M. S. de Vrij, S. A. Kushner, O. Harschnitz, D. van Riel, The neuroinvasiveness, neurotropism, and neurovirulence of SARS-CoV-2. *Trends in Neurosciences*. **45**, 358–368 (2022).

10. M. Prinz, J. Priller, The role of peripheral immune cells in the CNS in steady state and disease. *Nat Neurosci*. **20**, 136–144 (2017).

11. G. A. de Erausquin, H. Snyder, M. Carrillo, A. A. Hosseini, T. S. Brugha, S. Seshadri, CNS SARS-CoV-2 Consortium, The chronic neuropsychiatric sequelae of COVID-19: The need for a prospective study of viral impact on brain functioning. *Alzheimers Dement*. **17**, 1056–1065 (2021).

12. J. Meinhardt, J. Radke, C. Dittmayer, J. Franz, C. Thomas, R. Mothes, M. Laue, J. Schneider, S. Brünink, S. Greuel, M. Lehmann, O. Hassan, T. Aschman, E. Schumann, R. L. Chua, C. Conrad, R. Eils, W. Stenzel, M. Windgassen, L. Rößler, H.-H. Goebel, H. R. Gelderblom, H. Martin, A. Nitsche, W. J. Schulz-Schaeffer, S. Hakroush, M. S. Winkler, B. Tampe, F. Scheibe, P. Körtvélyessy, D. Reinhold, B. Siegmund, A. A. Kühl, S. Elezkurtaj, D. Horst, L. Oesterhelweg, M. Tsokos, B. Ingold-Heppner, C. Stadelmann, C. Drosten, V. M. Corman, H. Radbruch, F. L. Heppner, Olfactory transmucosal SARS-CoV-2 invasion as

a port of central nervous system entry in individuals with COVID-19. *Nat Neurosci*. **24**, 168–175 (2021).

13. S. D. Mhatre, C. A. Tsai, A. J. Rubin, M. L. James, K. I. Andreasson, Microglial malfunction: the third rail in the development of Alzheimer's disease. *Trends Neurosci*. **38**, 621–636 (2015).

14. J. Shanley, A. Valenciano, G. Timmons, V. Kakarla, A. Miner, T. Rempe, J. Graves, Longitudinal Evaluation of Neuro-PASC Symptoms (S8.007). *Neurology*. **98** (2022) (available at https://n.neurology.org/content/98/18_Supplement/732).

15. H. E. Davis, G. S. Assaf, L. McCorkell, H. Wei, R. J. Low, Y. Re'em, S. Redfield, J. P. Austin, A. Akrami, Characterizing long COVID in an international cohort: 7 months of symptoms and their impact. *EClinicalMedicine*. **38**, 101019 (2021).

16. G. G. Kovacs, E. Gelpi, Clinical Neuropathology Practice News 3-2012: the "ABC" in AD – revised and updated guideline for the neuropathologic assessment of Alzheimer's disease. *Clin Neuropathol*. **31**, 116–118 (2012).

17. M. Lampart, N. Zellweger, S. Bassetti, S. Tschudin-Sutter, K. M. Rentsch, M. Siegemund, R. Bingisser, S. Osswald, G. M. Kuster, R. Twerenbold, Clinical utility of inflammatory biomarkers in COVID-19 in direct comparison to other respiratory infections—A prospective cohort study. *PLOS ONE*. **17**, e0269005 (2022).

18. A. de Oliveira Matos, P. H. dos Santos Dantas, M. Figueira Marques Silva-Sales, H. Sales-Campos, The role of the triggering receptor expressed on myeloid cells-1 (TREM-1) in non-bacterial infections. *Critical Reviews in Microbiology*. **46**, 237–252 (2020).

19. S. Lee, Y. Yu, J. Trimpert, F. Benthani, M. Mairhofer, P. Richter-Pechanska, E. Wyler, D. Belenki, S. Kaltenbrunner, M. Pammer, L. Kausche, T. C. Firsching, K. Dietert, M. Schotsaert, C. Martínez-Romero, G. Singh, S. Kunz, D. Niemeyer, R. Ghanem, H. J. F. Salzer, C. Paar, M. Mülleder, M. Uccellini, E. G. Michaelis, A. Khan, A. Lau, M. Schönlein, A. Habringer, J. Tomasits, J. M. Adler, S. Kimeswenger, A. D. Gruber, W. Hoetzenecker, H. Steinkellner, B. Purfürst, R. Motz, F. Di Pierro, B. Lamprecht, N. Osterrieder, M. Landthaler, C. Drosten, A. García-Sastre, R. Langer, M. Ralser, R. Eils, M. Reimann, D. N. Y. Fan, C. A. Schmitt, Virus-induced senescence is a driver and therapeutic target in COVID-19. *Nature*. **599**, 283–289 (2021).

20. J.-P. Coppé, P.-Y. Desprez, A. Krtolica, J. Campisi, The senescence-associated secretory phenotype: the dark side of tumor suppression. *Annu Rev Pathol*. **5**, 99–118 (2010).

21. A. Margiotta, Role of SNAREs in Neurodegenerative Diseases. *Cells*. **10**, 991 (2021).

22. A. Manda-Handzlik, U. Demkow, The Brain Entangled: The Contribution of Neutrophil Extracellular Traps to the Diseases of the Central Nervous System. *Cells*. **8**, 1477 (2019).

23. R. Lugano, M. Ramachandran, A. Dimberg, Tumor angiogenesis: causes, consequences, challenges and opportunities. *Cell. Mol. Life Sci.* **77**, 1745–1770 (2020).

24. W. Jian, Z. Zhang, S. Chu, Y. Peng, N. Chen, Potential roles of brain barrier dysfunctions in the early stage of Alzheimer's disease. *Brain Research Bulletin*. **142**, 360–367 (2018).

25. T. Licht, E. Keshet, Delineating multiple functions of VEGF-A in the adult brain. *Cell. Mol. Life Sci.* **70**, 1727–1737 (2013).

26. S. Pasquin, M. Sharma, J.-F. Gauchat, Ciliary neurotrophic factor (CNTF): New facets of an old molecule for treating neurodegenerative and metabolic syndrome pathologies. *Cytokine & Growth Factor Reviews*. **26**, 507–515 (2015).

27. M. Amidfar, J. de Oliveira, E. Kucharska, J. Budni, Y.-K. Kim, The role of CREB and BDNF in neurobiology and treatment of Alzheimer's disease. *Life Sciences*. **257**, 118020 (2020).

28. W. Z. Eu, Y.-J. Chen, W.-T. Chen, K.-Y. Wu, C.-Y. Tsai, S.-J. Cheng, R. N. Carter, G.-J. Huang, The effect of nerve growth factor on supporting spatial memory depends upon hippocampal cholinergic innervation. *Transl Psychiatry*. **11**, 1–13 (2021).

29. H. Ikeshima-Kataoka, C. Sugimoto, T. Tsubokawa, Integrin Signaling in the Central Nervous System in Animals and Human Brain Diseases. *International Journal of Molecular Sciences*. **23**, 1435 (2022).

30. Y. Zhou, J. Xu, Y. Hou, J. B. Leverenz, A. Kallianpur, R. Mehra, Y. Liu, H. Yu, A. A. Pieper, L. Jehi, F. Cheng, Network medicine links SARS-CoV-2/COVID-19 infection to brain microvascular injury and neuroinflammation in dementia-like cognitive impairment. *Alz Res Therapy*. **13**, 110 (2021).

31. A. R. Tröscher, I. Wimmer, L. Quemada-Garrido, U. Köck, D. Gessl, S. G. S. Verberk, B. Martin, H. Lassmann, C. G. Bien, J. Bauer, Microglial nodules provide the environment for pathogenic T cells in human encephalitis. *Acta Neuropathol*. **137**, 619–635 (2019).

32. T. Fischer-Smith, S. Croul, A. E. Sverstiuk, C. Capini, D. L'Heureux, E. G. Régulier, M. W. Richardson, S. Amini, S. Morgello, K. Khalili, J. Rappaport, CNS invasion by CD14+/CD16+ peripheral blood-derived monocytes in HIV dementia: perivascular accumulation and reservoir of HIV infection. *Journal of NeuroVirology*. **7**, 528–541 (2001).

546 33. L. Wang, P. B. Davis, N. D. Volkow, N. A. Berger, D. C. Kaelber, R. Xu, Association of
547 COVID-19 with New-Onset Alzheimer's Disease. *Journal of Alzheimer's Disease*. **89**, 411–
548 414 (2022).

549 34. I. Rutkai, M. G. Mayer, L. M. Hellmers, B. Ning, Z. Huang, C. J. Monjure, C. Coyne, R.
550 Silvestri, N. Golden, K. Hensley, K. Chandler, G. Lehmicke, G. J. Bix, N. J. Maness, K.
551 Russell-Lodrigue, T. Y. Hu, C. J. Roy, R. V. Blair, R. Bohm, L. A. Doyle-Meyers, J.
552 Rappaport, T. Fischer, Neuropathology and virus in brain of SARS-CoV-2 infected non-
553 human primates. *Nat Commun*. **13**, 1745 (2022).

554 35. M. Patarroyo, J. Prieto, J. Rincon, T. Timonen, C. Lundberg, L. Lindbom, B. Asjo, C. G.
555 Gahmbekg, Leukocyte-Cell Adhesion: A Molecular Process Fundamental in Leukocyte
556 Physiology. *Immunological Reviews*. **114**, 67–108 (1990).

557 36. T. M. Bui, H. L. Wiesolek, R. Sumagin, ICAM-1: A master regulator of cellular responses in
558 inflammation, injury resolution, and tumorigenesis. *Journal of Leukocyte Biology*. **108**, 787–
559 799 (2020).

560 37. G. E. Serrano, J. E. Walker, R. Arce, M. J. Glass, D. Vargas, L. I. Sue, A. J. Intorcia, C. M.
561 Nelson, J. Oliver, J. Papa, A. Russell, K. E. Suszczewicz, C. I. Borja, C. Belden, D.
562 Goldfarb, D. Shprecher, A. Atri, C. H. Adler, H. A. Shill, E. Driver-Dunckley, S. H. Mehta,
563 B. Readhead, M. J. Huentelman, J. L. Peters, E. Alevritis, C. Bimi, J. P. Mizgerd, E. M.
564 Reiman, T. J. Montine, M. Desforges, J. L. Zehnder, M. K. Sahoo, H. Zhang, D. Solis, B. A.
565 Pinsky, M. Deture, D. W. Dickson, T. G. Beach, *medRxiv*, in press,
566 doi:10.1101/2021.02.15.21251511.

38. S. M. Burks, H. Rosas-Hernandez, M. Alejandro Ramirez-Lee, E. Cuevas, J. C. Talpos, Can SARS-CoV-2 infect the central nervous system via the olfactory bulb or the blood-brain barrier? *Brain, Behavior, and Immunity*. **95**, 7–14 (2021).

39. R. M. Parodi-Rullán, S. Javadov, S. Fossati, Dissecting the Crosstalk between Endothelial Mitochondrial Damage, Vascular Inflammation, and Neurodegeneration in Cerebral Amyloid Angiopathy and Alzheimer's Disease. *Cells*. **10**, 2903 (2021).

40. P. Xu, Y. Hong, Y. Xie, K. Yuan, J. Li, R. Sun, X. Zhang, X. Shi, R. Li, J. Wu, X. Liu, W. Hu, W. Sun, TREM-1 Exacerbates Neuroinflammatory Injury via NLRP3 Inflammasome-Mediated Pyroptosis in Experimental Subarachnoid Hemorrhage. *Transl. Stroke Res.* **12**, 643–659 (2021).

41. J. D. Lünemann, S. Malhotra, M. L. Shinohara, X. Montalban, M. Comabella, Targeting Inflammasomes to Treat Neurological Diseases. *Annals of Neurology*. **90**, 177–188 (2021).

42. F. J. Herman, G. M. Pasinetti, Principles of inflammasome priming and inhibition: Implications for psychiatric disorders. *Brain Behav Immun*. **73**, 66–84 (2018).

43. G. R. Campbell, R. K. To, J. Hanna, S. A. Spector, SARS-CoV-2, SARS-CoV-1, and HIV-1 derived ssRNA sequences activate the NLRP3 inflammasome in human macrophages through a non-classical pathway. *iScience*. **24**, 102295 (2021).

44. R. C. Smail, B. J. Brew, HIV-associated neurocognitive disorder. *Handb Clin Neurol*. **152**, 75–97 (2018).

45. X. Sun, H. Zhang, D. Yao, Y. Xu, Q. Jing, S. Cao, L. Tian, C. Li, Integrated Bioinformatics Analysis Identifies Hub Genes Associated with Viral Infection and Alzheimer's Disease. *Journal of Alzheimer's Disease*. **85**, 1053–1061 (2022).

589 46. E. Tavazzi, D. Morrison, P. Sullivan, S. Morgello, T. Fischer, Brain inflammation is a
590 common feature of HIV-infected patients without HIV encephalitis or productive brain
591 infection. *Curr HIV Res*. **12**, 97–110 (2014).

592 47. H. Varet, L. Brillet-Guéguen, J.-Y. Coppée, M.-A. Dillies, SARTools: A DESeq2- and
593 EdgeR-Based R Pipeline for Comprehensive Differential Analysis of RNA-Seq Data. *PLOS*
594 *ONE*. **11**, e0157022 (2016).

595 48. A. Krämer, J. Green, J. Pollard Jr, S. Tugendreich, Causal analysis approaches in Ingenuity
596 Pathway Analysis. *Bioinformatics*. **30**, 523–530 (2014).

597 49. R. Edgar, M. Domrachev, A. E. Lash, Gene Expression Omnibus: NCBI gene expression
598 and hybridization array data repository. *Nucleic Acids Res*. **30**, 207–210 (2002).

599

600

Acknowledgments

The authors thank the Neuropathology Brain Bank and Research CoRE of the Icahn School of Medicine at Mount Sinai for postmortem samples.

Funding:

The research was supported by Unrestricted Funds and Altschul Foundation (GMP)

National Institutes of Health Office of Research Infrastructure Programs grant P51OD01110 (TF)

The content is solely the responsibility of the authors and does not necessarily represent the official views of the National Institutes of Health and Veteran Administration

Author contributions:

Conceptualization: EG, GMP

Methodology: EG, TF, GP

Investigation: EG, KT, SN, LH, ME, GH, BM, NJ, TF

Visualization: EG, ME, LS, LH, TF

Supervision: TF, GMP

Writing—original draft: EG, ME, TF

Writing—review & editing: EG, SN, NJ, TF, GMP

Competing interests: NJ receives grant funding paid to her institution from NINDS (NIH U24NS107201, NIH IU54NS100064, 3R01CA202911-05S1, R21NS122389, R01HL161847). Some of these grants are COVID-19 related but focus on the neuroimaging findings. The other authors declare that they have no conflict of interest with the contents of this article.

626

627 **Data and materials availability:** The authors declare that the data supporting the findings
628 of this study are available within the paper and its supplementary information files. The
629 raw data discussed in this publication will be accessible through NCBI's Gene Expression
630 Ominubus (GEO) upon publication (*49*).

Figures and Tables

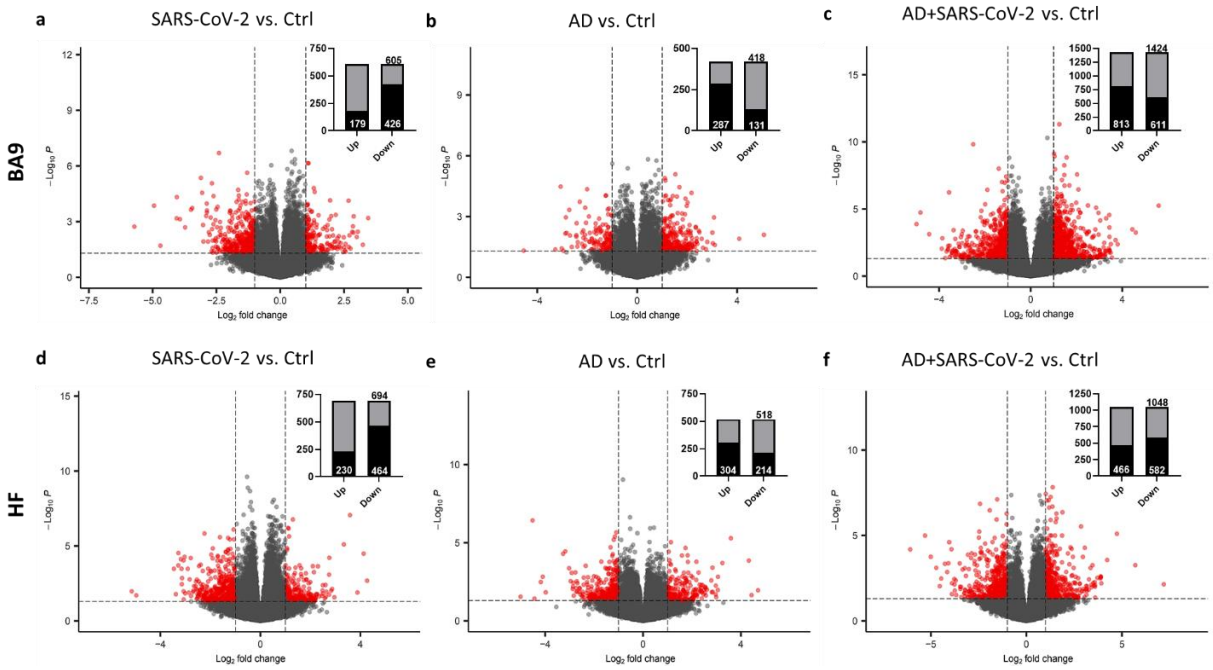

Fig. 1. Gene expression in cortical BA9 and HF tissue.
Volcano plot distribution of gene transcripts of the cortical BA9 region in as shown in **A**, SARS-CoV-2 cases, in **B,** AD cases, and in **C**, SARS-CoV-2 infected AD cases compared to neurological control cases. The HF region in panels **D**, SARS-CoV-2 cases, **E**, AD cases, and **F** SARS-CoV-2 infected AD cases compared to neurological control cases. Volcano plots were generated from 39,901 genes in A, B, D and E, and 38,021 genes in C 35,527 genes in F. Transcripts with nominal $p<0.01$ and an absolute log fold-change (logFC) greater than 1 are indicated in red and shown in inlayed bar graphs wherein the number of upregulated and downregulated genes are indicated in black as part of the total of differentially regulated genes (grey).

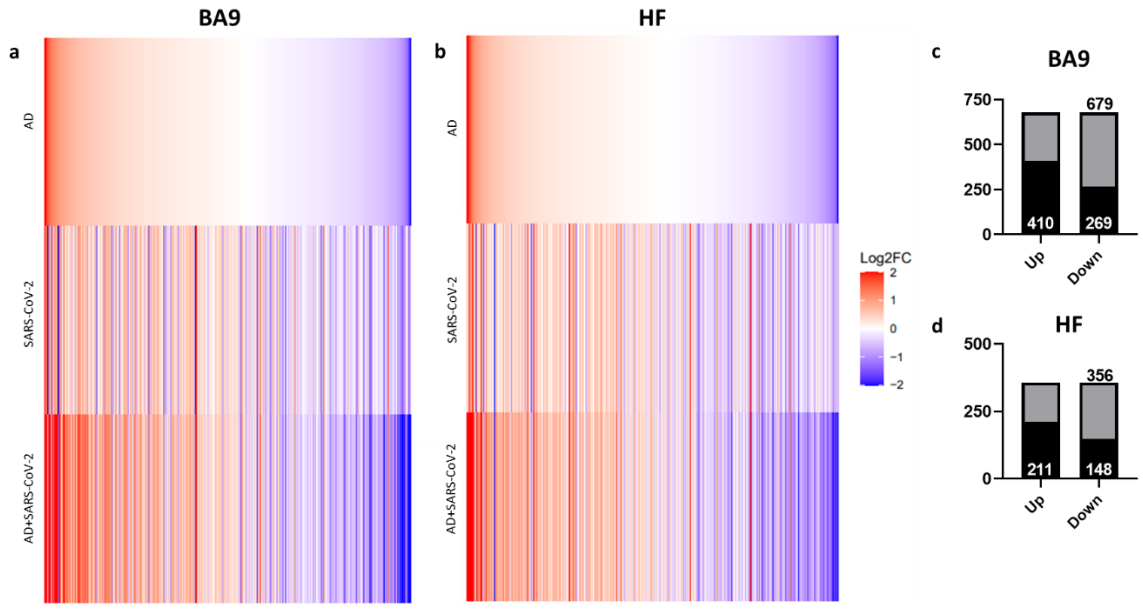

Fig. 2. Similarity of gene expression in cortical BA9 and HF tissue in SARS-CoV-2 and SARS-CoV-2 infected AD relative to AD individuals based on log2FC.
Genes known to be differentially expressed due to either SARS-CoV-2 infection or AD were examined with respect to their gene expression changes, with the given gene set being selected for cortical BA9, shown in panel **A**, or HF, shown in panel **B**. The log2FC of the genes for three individual differential comparisons (AD versus Control, SARS-CoV-2 versus Control, and SARS-CoV-2 infected AD versus Control) are shown for the BA9 and HF tissue as shown in panels A and B, respectively. Then, using Ingenuity pathway analysis (IPA) as a filtering system for genes within the database, we compared the similarity in expression of genes present in all datasets (SARS-CoV-2, AD and SARS-CoV-2 infected AD cases), shown in panel **C** and **D**, in both the cortical BA9 and HF.

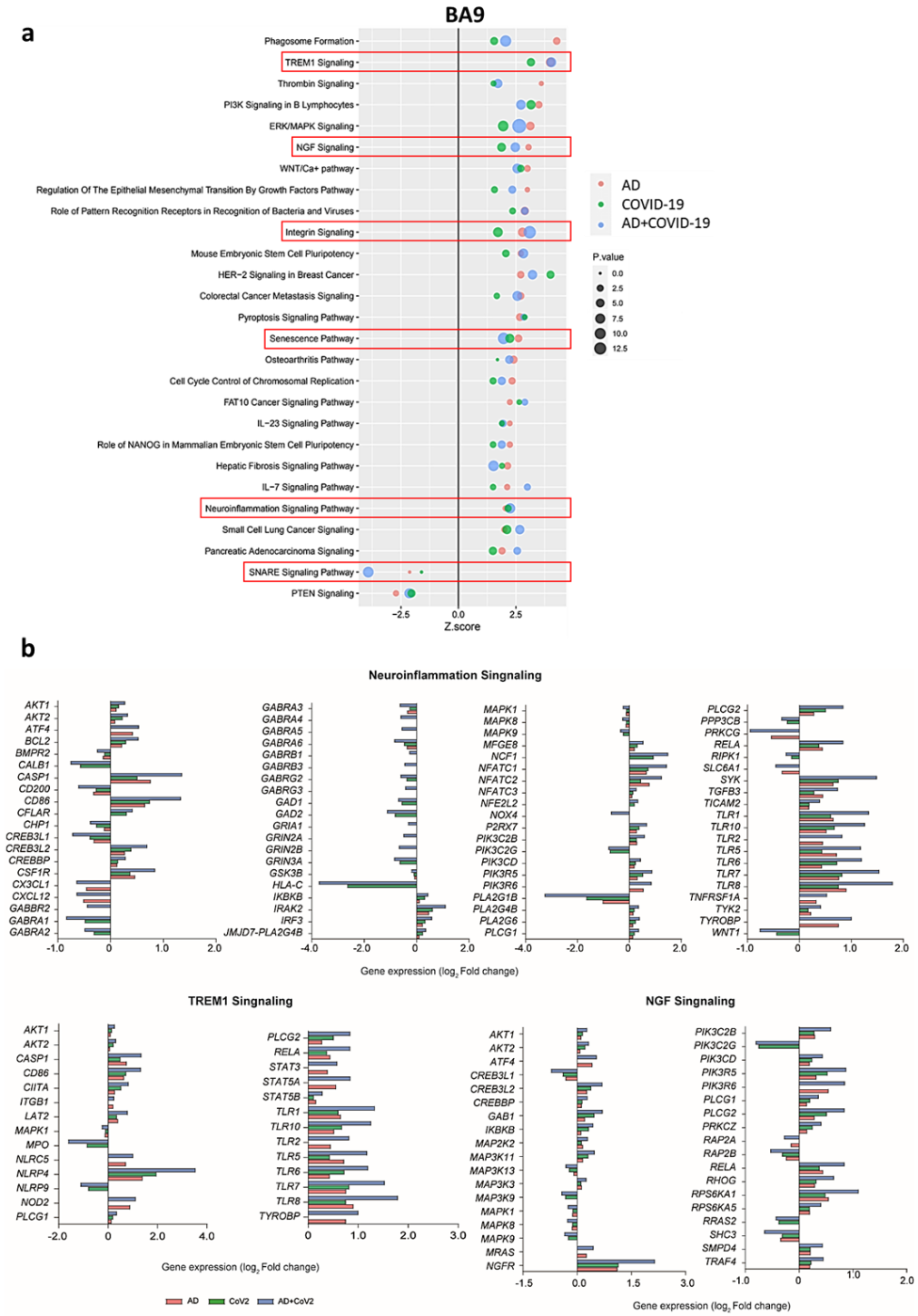

Fig. 3. Changes in Signaling Pathways within the cortical BA9.
Canonical Pathway Similarities as seen in panel **A**, show top regulated canonical pathways within the cortical BA9 in SARS-CoV-2, AD, and SARS-CoV-2 infected AD cases in reference to the control. Activation score (Z-score) is shown on the X-axis, while the pathways are indicated on the Y-axis. The color of the points indicates the IPA comparison, while the size of the point represents the -log10 p-value of the IPA comparison, with the larger points indicating the lowest p-values. The predicted gene regulation of the Neuroinflammation, TREM1 and NGF pathways, shown in panel **B**, indicate that SARS-CoV-2, AD and SARS-CoV-2 infected AD groups have similar expression in key inflammatory and neuronal pathways.

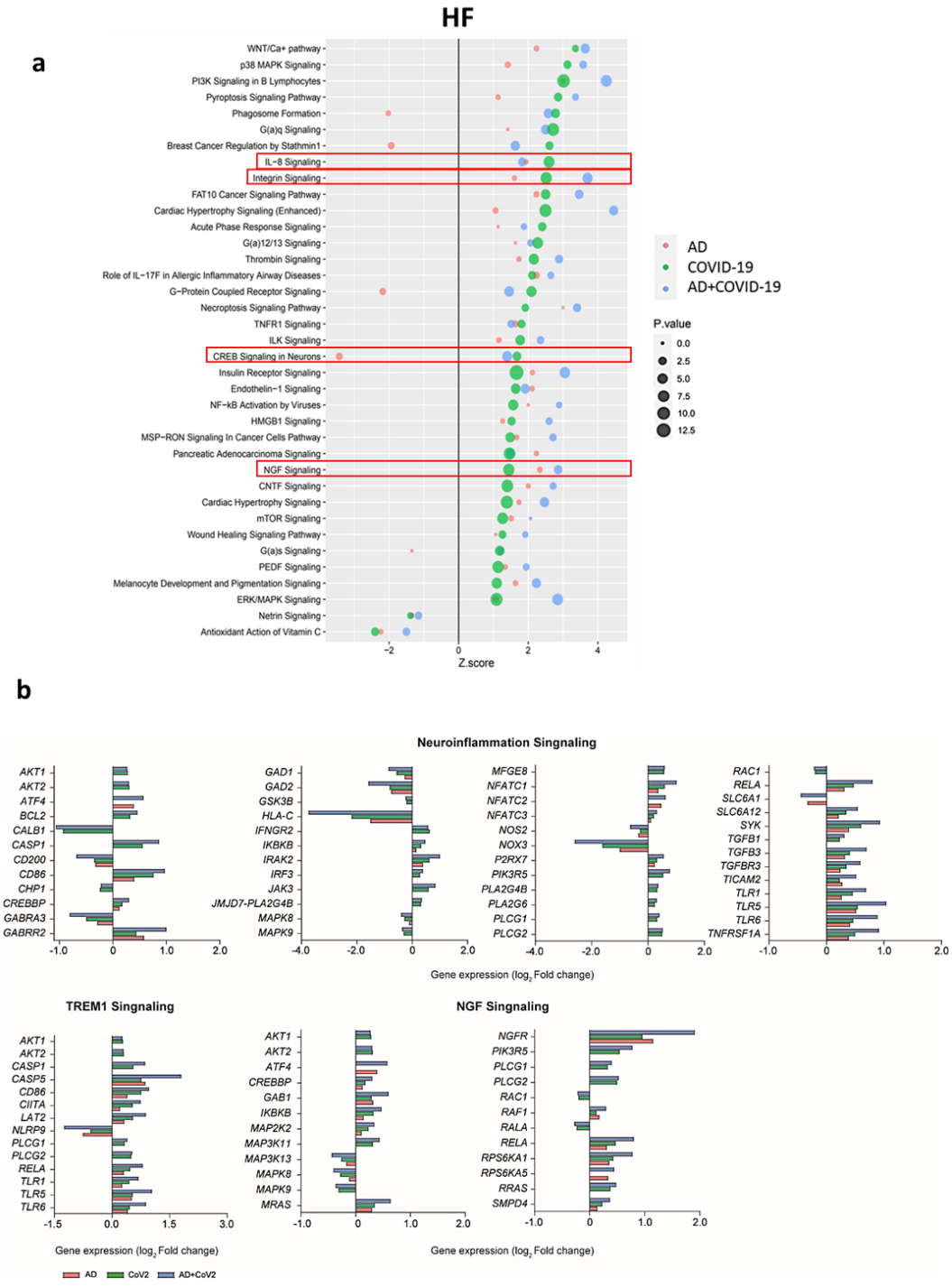

Fig. 4. Changes in Signaling Pathways within the HF.
Canonical pathway similarities as seen in panel **A**, top regulated canonical pathways were compared within the HF in SARS-CoV-2, AD, and SARS-CoV-2 infected AD cases in reference to the control. Activation score (Z-score) is shown on the X-axis, while the pathways are indicated on the Y-axis. The color of the points indicates the IPA comparison, while the size of the point represents the -log10 p-value of the IPA comparison, with the larger points indicating the lowest p-values. The predicted gene regulation of the Neuroinflammation, TREM1 and NGF pathways, shown in panel **B**, indicate that SARS-CoV-2, AD and SARS-CoV-2 infected AD groups have similar expression in key inflammatory and neuronal pathways.

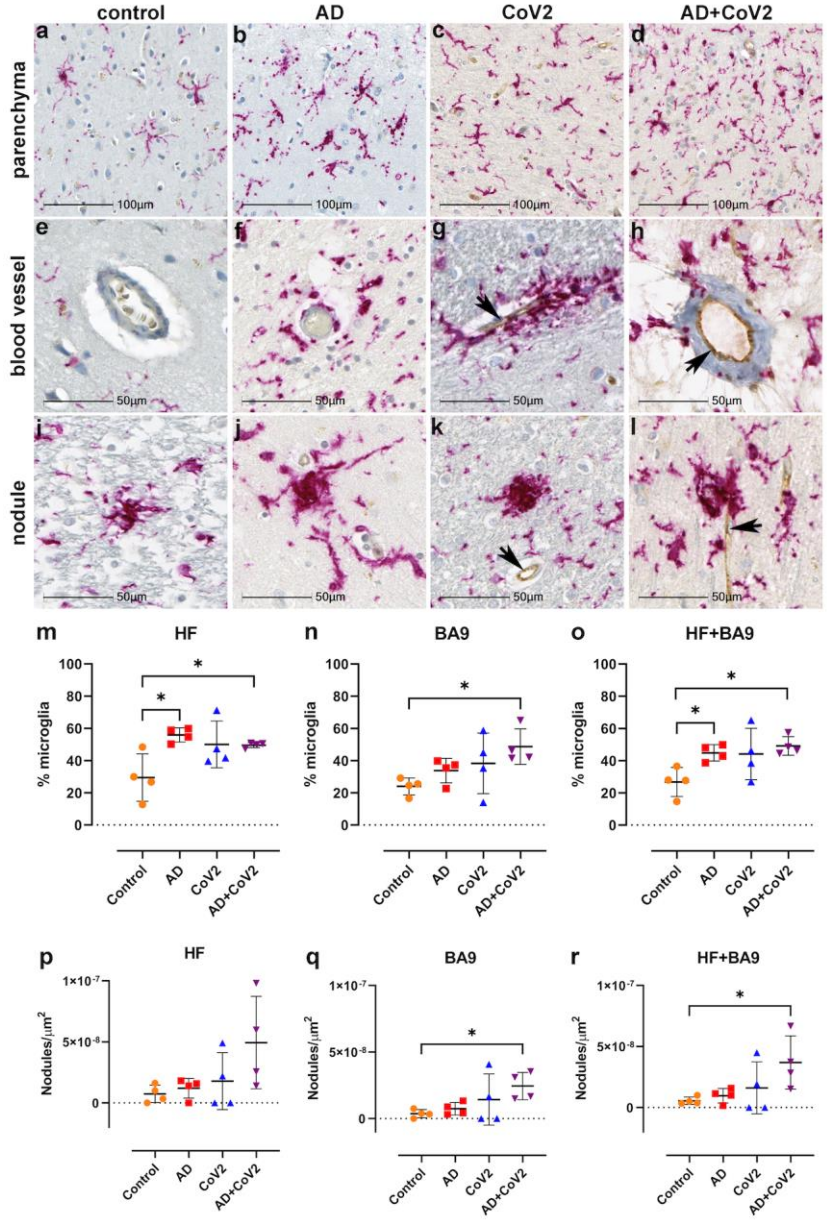

Fig. 5. Microgliosis and nodular lesions in neurological controls, SARS-CoV-2, AD and SARS-CoV-2 infected individuals.

The level of microglial activation was assessed by immunohistochemical staining using anti-Iba-1 antibody with Vector Red. The presence of SARS-CoV-2 was assessed using an antibody against the virus nucleocapsid and visualized with DAB. Parenchymal microglia are more frequent and highly activated in the context of infection with and without AD, as shown by thickened processes, enlarged soma, and loss of individual cellular domain in panels **B-D**, as compared to age-matched controls shown in **A and E**. When present, SARS-CoV-2 localizes to the blood vessel endothelium shown in panels **G, H, K, L** (black arrows). Microglia appear to gather around blood vessels in disease but do not form cuffs (**F, G, H**). Nodular lesions are seen in most cases assessed, regardless of disease status (**I-L**), however, they appear larger and more frequent in the context of disease shown in panels **J-L**, as compared to controls, panel **I**. A multiplex algorithm was used to count all cells, using DAPI+ nuclei, with HALO and calculate percent frequency of Iba-1+ microglia, shown in panels **M-O**. There was upregulation of Iba-1 in the hippocampus as compared to the cortical BA9 region for most cases, though there is a significantly higher ratio of microglia relative to other cells when comparing the AD and SARS-CoV-2 infected AD cases to

the control group shown in panel **M**. This trend seems to hold true for cortical BA9 region as well, where the only groups with a significant difference in microglia ratios are the control and SARS-CoV-2 infected AD cases shown in panel **N**. When all cases have both regions averaged, the level of microgliosis is shown to be higher in the AD and SARS-CoV-2 infected AD cases when compared to control in panel **O**. Graphs **P-R** show the normalized counts of microglial nodule frequency. A higher frequency of nodules is seen in the HF, however, the difference between groups did not reach statistical significance as shown in panel **P**. In contrast, fewer nodules are seen in cortical BA9, overall. A statistically significant higher number of lesions are seen in SARS-CoV-2 infected AD cases, as compared to control cortical BA9, suggesting greater inflammation in the cortical BA9 of patients with both AD and SARS-CoV-2 infection, shown in panel **Q**. Significance was maintained between the control and SARS-CoV-2 infected AD groups when the average was taken for both brain regions per case shown in panel **R**. Statistics were performed with a two-tailed Mann-Whitney U test. *$p<0.05$. Data are expressed as mean ± SEM.

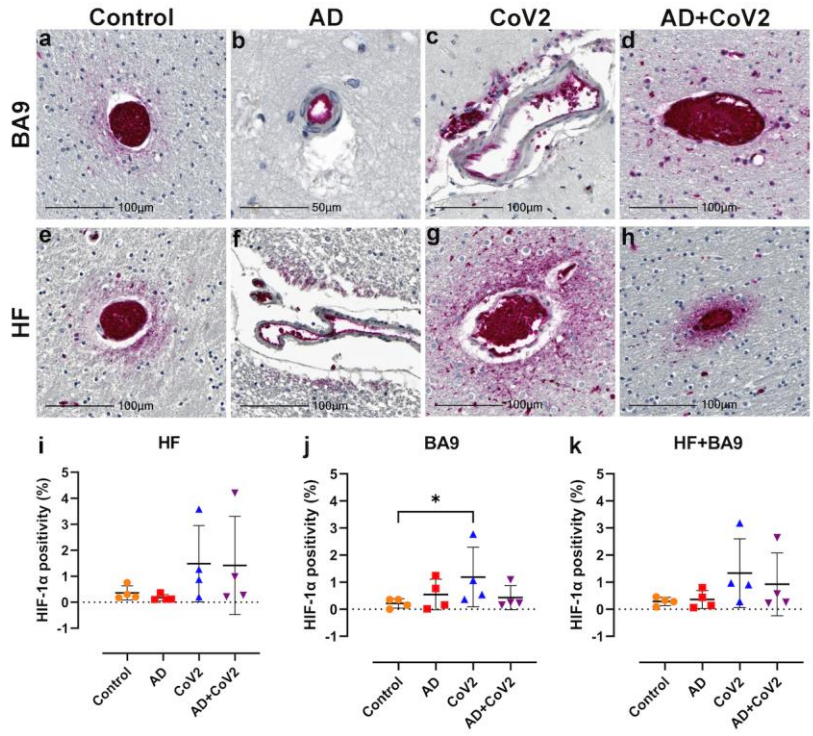

Fig. 6. Hypoxia-inducible factor-1 alpha subunit (HIF-1α) in neurological controls, SARS-CoV-2, AD and SARS-CoV-2 infected individuals.

Representative images demonstrate HIF-1α immunopositivity around the vasculature that extends into the parenchyma in brain of patients with SARS-CoV-2 infection, regardless of AD status shown in panels **C, D, G, H**. Comparatively, this is seen less frequently and does not extend significantly into the parenchyma in brain of age-matched controls, shown in panels **A and E**. In AD only, positivity was most often observed in epithelium with no or minimal extension into the brain parenchyma as shown in panels **B and F**. Graphs show the total percentage of tissue positive for HIF-1α, as defined using a HALO area algorithm for detection of Vector Red intensity over the whole section shown (**I-K**). Although statistical significance between groups was not reached in the HF or averaged group comparisons, increased HIF-1α expression is seen in the SARS-CoV-2 infected patients, with and without AD, as compared to age-matched controls in panels **I and K**. An increase in area positivity is seen in all groups in the cortical BA9 region, as compared to non-affected controls, however, statistical significance is only seen with the SARS-CoV-2 group in panel **J**. Statistics were performed with a two-tailed Mann-Whitney U test. *$p<0.05$. Data are expressed as mean ± SEM.